Towards Rapid Prototyping and Comparability in Active Learning for Deep Object Detection

Tobias Riedlinger[1,*,a], Marius Schubert[2,*,b], Karsten Kahl[2,c], Hanno Gottschalk[1,d] and Matthias Rottmann[2,e]

[1] *Institute of Mathematics, Technical University Berlin, Germany*

[2] *School of Mathematics and Natural Sciences, IZMD, University of Wuppertal, Germany*

Keywords: Active Learning, Deep Object Detection, Prototyping.

Abstract: Active learning as a paradigm in deep learning is especially important in applications involving intricate perception tasks such as object detection where labels are difficult and expensive to acquire. Development of active learning methods in such fields is highly computationally expensive and time consuming which obstructs the progression of research and leads to a lack of comparability between methods. In this work, we propose and investigate a sandbox setup for rapid development and transparent evaluation of active learning in deep object detection. Our experiments with commonly used configurations of datasets and detection architectures found in the literature show that results obtained in our sandbox environment are representative of results on standard configurations. The total compute time to obtain results and assess the learning behavior can be reduced by factors of up to 14 compared to Pascal VOC and up to 32 compared to BDD100k. This allows for testing and evaluating data acquisition and labeling strategies in under half a day and contributes to the transparency and development speed in the field of active learning for object detection.

1 INTRODUCTION

Deep learning requires large amounts of data, typically annotated by vast amounts of human labor (Zhan et al., 2022; Budd et al., 2021; Li and Sethi, 2006). In particular in complex computer vision tasks such as object detection (OD), the amount of labor per image can lead to substantial costs for data labeling. Therefore, it is desirable to avoid unnecessary labeling effort and to have a rather large variability of the database. *Active learning* (AL, see e.g., (Settles, 2009)) is one of the key methodologies that aims at labeling the data that matters for learning. AL *alternates model training and data labeling* as illustrated in Fig. 1. At the core of each AL method is a query strategy that decides post-training which unlabeled data to query for labeling. The computation cost of AL is in general at least an order of magnitude higher than ordinary model training and so is its development (Tsvigun et al., 2022; Li and Sethi, 2006), which comprises several AL experiments of T query steps with different parameters, ablation studies, etc. Hence, it is *notoriously challenging to develop new AL methods* for applications where model training itself is already computationally costly. In the field of

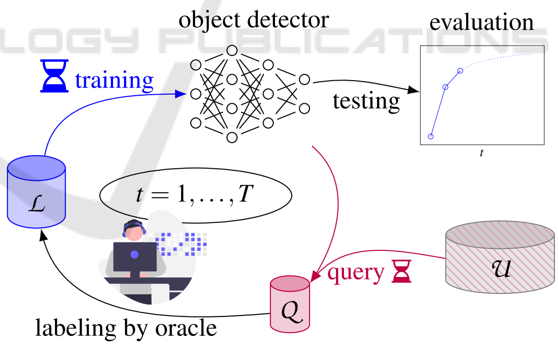

Figure 1: The generic pool-based AL cycle consisting of training on labeled data $\mathcal{L}$, querying informative data points $\mathcal{Q}$ out of a pool of unlabeled data $\mathcal{U}$ and annotation by a (human) oracle. In practice, training compute time is orders of magnitude larger than evaluating the AL strategy itself or the query step.

[a] https://orcid.org/0000-0002-1953-8607
[b] https://orcid.org/0000-0002-9410-8949
[c] https://orcid.org/0000-0002-3510-3320
[d] https://orcid.org/0000-0003-2167-2028
[e] https://orcid.org/0000-0003-3840-0184
[*] Equal contribution.

Riedlinger, T., Schubert, M., Kahl, K., Gottschalk, H. and Rottmann, M.
Towards Rapid Prototyping and Comparability in Active Learning for Deep Object Detection.
DOI: 10.5220/0012315400003660

In *Proceedings of the 19th International Joint Conference on Computer Vision, Imaging and Computer Graphics Theory and Applications (VISIGRAPP 2024) - Volume 2: VISAPP*, pages 366-374
ISBN: 978-989-758-679-8; ISSN: 2184-4321

OD, a number of works overcame this cumbersome hurdle (Yoo and Kweon, 2019; Brust et al., 2018; Roy et al., 2018; Haussmann et al., 2020; Schmidt et al., 2020; Choi et al., 2021; Yuan et al., 2021; Elezi et al., 2022; Papadopoulos et al., 2017; Desai et al., 2019; Subramanian and Subramanian, 2018). However, these works did so in *highly inhomogeneous settings which makes their comparison difficult*. Besides that, AL with real-world data may suffer from other influencing factors, e.g., the quality of labels to which end fundamental research is conducted on AL in presence of label errors (Bouguelia et al., 2015; Bouguelia et al., 2018; Younesian et al., 2020; Younesian et al., 2021). These observations demand for a development environment enabling rapid prototyping, cutting down the huge computational efforts of AL in OD and fostering comparability and transparency.

Contribution. In this work, we propose a development environment that drastically cuts down the computational cost of developing AL methods. To this end, we construct (a) two datasets that generalize MNIST (LeCun et al., 1998) and EMNIST (Cohen et al., 2017) to the setting of OD making use of background images from MS-COCO (Lin et al., 2014) and (b) a selection of suitable small-scale models. We conduct experiments showing that results on our datasets generalize to a similar degree to complex real-world datasets like Pascal VOC (Everingham et al., 2010) or BDD100k (Yu et al., 2020), as they generalize among each other. We also demonstrate a reduction of computational effort of AL experiments by factors of up to 32. Further, a nuanced evaluation protocol is introduced in order to prevent wrong conclusions from misleading evidence encountered in experiments. We summarize our contributions as follows:

- We propose a *sandbox environment* with two datasets, three network architectures, several AL baselines and an evaluation protocol. This allows for broad, detailed and transparent comparisons at lowered computational effort.
- We analyze the *generalization ability* of our sandbox in terms of AL rank correlations. We find similar performance progressions indicating that results obtained by our sandbox generalize well to Pascal VOC and BDD100k, i.e., to the same extent as results generalize between Pascal VOC and BDD100k.
- We contribute to future AL development by providing an implementation of our pipeline in a flexible environment as well as an *automated framework for evaluation and visualization of results*. This involves configurations with hyperparameters, as well as checkpoints and seeded experimental results (see https://github.com/tobiasriedlinger/al-rapid-prototyping).

The remainder of this work is structured as follows: Section 2 contains a summary of the literature in fully-supervised AL for OD and explains how the present work relates to it. In Section 3 we introduce our motivation, methods investigated and our proposed evaluation metrics. Section 4 first introduces our experimental setup. We investigate the comparability of AL methods in OD in different cases. Afterwards, we compute rank correlations for different datasets to measure the degree of similarity between the AL results for different datasets. Finally, we show time measurements to estimate the speed-ups achieved. We close with concluding remarks which we draw from the empirical evidence in Section 5.

2 RELATED WORK

Numerous methods of AL have been developed in the classification setting (Settles, 2009) and largely fall into the categories of uncertainty-based and diversity-based query strategies. While uncertainty methods make use of the current model's prediction, diversity methods exploit the annotated dataset together with the current model and seek representative coverage of the data generating distribution. Due to increased complexity in annotations in OD, AL plays a large role in OD which has been addressed by some authors. (Yoo and Kweon, 2019) present a task-agnostic method based on a loss estimation module. (Brust et al., 2018) estimate prediction-wise uncertainty by the probability margin and aggregate to image uncertainty in different ways. (Roy et al., 2018) follow a similar idea using classification entropy. Moreover, a white-box approach similar to query-by-committee in introduced. (Haussmann et al., 2020) utilize ensembles to estimate classification uncertainty via mutual information while (Schmidt et al., 2020) use combinations of localization and classification uncertainty. But in particular, as training a variety of detector heads in each step is very costly, ensemble query methods tend to be approximated by Monte Carlo (MC) Dropout (Gal and Ghahramani, 2016; Gal et al., 2017). Other works investigate special AL-adapted OD architectures or loss functions (Choi et al., 2021; Yuan et al., 2021). In this paper we *compare uncertainty-based methods with each other that are exclusively based on fully supervised training of non-adapted object detectors* (Brust et al., 2018; Roy et al., 2018; Haussmann et al., 2020; Choi et al., 2021). The preceding literature is difficult to compare since datasets, models, frameworks and hyperparame-

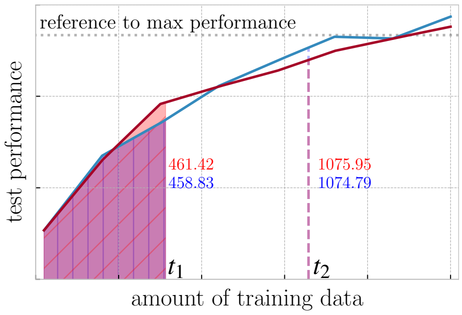

Figure 2: Area under AL curve (*AUC*) metric at different stages of an AL curve for two different query strategies (averaged, taken from experiments in Fig. 5).

ters for training and inference heavily differ from each other. Unlike the works mentioned, we aim at putting the AL task itself on equal footing between different settings to improve development speed and evaluation transparency. In our work, we compare a selection of the above-mentioned methods to each other with equivalent configurations for frequently used datasets and architectures. Comparative investigations of this kind has escaped previous research in the field.

3 A SANDBOX ENVIRONMENT WITH DATASETS, MODELS AND EVALUATION METRICS

In this section we describe the objective of AL and our sandbox environment. The main setting we propose consists of *two semi-synthetic OD datasets and down-scaled versions of standard OD models* leaving the detection mechanism unchanged. Additionally, we introduce evaluations capturing different aspects of the observed AL curve.

Active Learning. The term active learning refers to a setup (cf. Fig. 1) where only a limited amount of fully annotated data $\mathcal{L}$ is available together with a task-specific model. In addition, there is a pool (or a stream, however, we focus on pool-based AL) of unlabeled data $\mathcal{U}$ from which the model queries those samples $\mathcal{Q}$ which are most informative. Afterwards, $\mathcal{Q}$ is annotated by an oracle, which in practice is usually a human worker, added to $\mathcal{L}$ and the model is fine-tuned or fitted from scratch again. Success of the query strategy is measured by *observing an increase in test performance after training* on $\mathcal{L} \cup \mathcal{Q}$. Evaluation of the current model performance measured before each query step leads to graphs like the ones shown in Fig. 2. Querying data can take diverse algorithmic forms, see some of the methods described in Section 2 or (Settles, 2009).

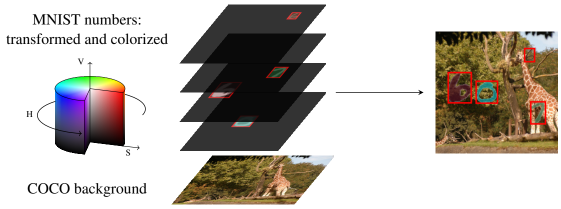

Figure 3: Generation scheme of semi-synthetic OD data from MNIST digits on a non-trivial background image from MS-COCO.

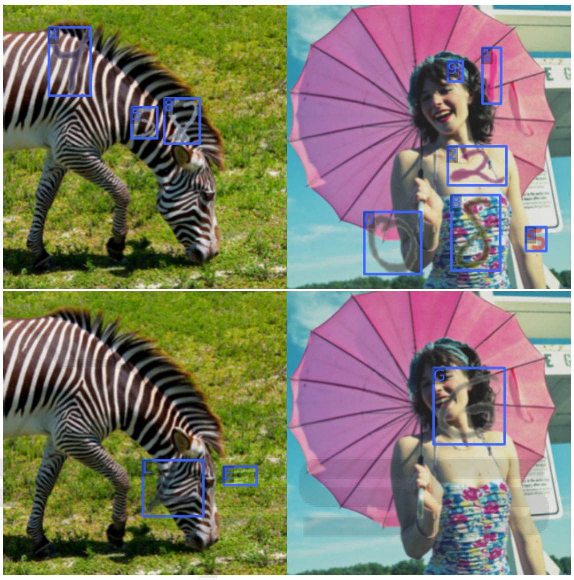

Figure 4: Dataset samples from MNIST-Det (top) and EMNIST-Det (bottom) including annotations.

Datasets. We construct an OD problem by building a synthetic overlay to images from the real-world MS-COCO dataset (cf. Fig. 3), which constitutes the data of our sandbox, see Fig. 4 for samples. COCO images with deleted annotations provide a realistic, feature-rich background on which foreground objects are spawned to be recognized. We utilize two sets of foreground categories: MNIST digits and EMNIST letters. We apply randomized coloration (uniform $(h,s,v) \sim U([0.0,1.0] \times [0.05,1.0] \times [0.1,1.0])$) and opacity ($\alpha \sim U([0.5,0.9])$) to foreground instances such that trivial edge detection becomes unfeasible. In addition, we apply image translation, scaling and shearing to all numbers/letters. The number of instances per background image is Poisson-distributed with mean $\lambda = 3$. Tight bounding box (and instance segmentation) annotations are obtained from the original transformed gray scale versions and the category label are inherited. Compared to simple OD datasets such as SVHN (Netzer et al., 2011), the geometric variety in our datasets is more similar to those of large OD benchmarks such as Pascal VOC or MS-COCO,

Table 1: Standard deviations of center coordinates, width and height (all relative to image size) of bounding boxes, as well, as number of categories in the training split for several object detection datasets.

Dataset	c_x	c_y	w	h	# categories
SVHN	0.099	0.059	0.048	0.161	10
Pascal VOC	0.217	0.163	0.284	0.277	20
MS COCO	0.254	0.209	0.220	0.234	80
KITTI	0.229	0.080	0.067	0.157	8
BDD100k	0.224	0.133	0.059	0.086	10
MNIST-Det	0.233	0.233	0.054	0.054	10
EMNIST-Det	0.233	0.233	0.066	0.065	26

Table 2: Exemplary OD architectures with backbone configurations employed in the experiments and associated number of parameters.

Detector	Backbone	# params	Backbone	# params
RetinaNet	ResNet50	36.5M	ResNet18	20.1M
Faster R-CNN	ResNet101	60.2M	ResNet18	28.3M
YOLOv3	Darknet53	61.6M	Darknet20	10.3M

see Table 1. The reduction in the dataset complexity allows for high performance even for small architectures and leads to quickly converging training and low inference times. In the following we term these datasets "MNIST-Det" and "EMNIST-Det".

Models. Modern OD architectures utilize several conceptually different mechanisms to solve the detection task. Irrespective of the amount of accessible data, some applications of OD may require high inference speed while others may require a large degree of precision or some trade-off between the two. The underlying detection mechanism is, however, disjoint to some degree from the depth of the backbone. The latter is mainly responsible for the quality and resolution of features. We use models with reduced network depth while keeping the detection head unchanged. Table 2 shows the choices for a YOLOv3 (Redmon and Farhadi, 2018), RetinaNet (Lin et al., 2017) and Faster R-CNN (Ren et al., 2015) setup, which we have adapted. The parameter count is reduced by up to a factor of around 6 leading to a significant decrease in training and inference time.

Active Learning Methods in Object Detection. The frequently used uncertainty-based query strategies from image classification, such as entropy, probability margin, MC dropout, and mutual information, determine instance-specific but not image-wise scores. However, the query strategies here involve image-wise selection for annotation. It is, therefore, useful to introduce an aggregation step like in (Brust et al., 2018) to obtain image-wise query scores.

For a given image $\mathbf{x}$, a neural network predicts a fixed number N of bounding boxes

$$\hat{b}_{\mathbf{x}}^{(i)} = \{x_{\min}, y_{\min}, x_{\max}, y_{\max}, s, p_1, \ldots, p_C\}, \qquad (1)$$

where $i = 1, \ldots, N$, $x_{\min}, y_{\min}, x_{\max}, y_{\max}$ represent the localization, s the objectness score (or analog) and $p_1, \ldots, p_C$ the class probabilities for the C classes. Only the set of boxes post-non-maximum-suppression (NMS) and score thresholding are used to determine prediction uncertainties. The choice of threshold parameters for NMS significantly influences the queries, since they decide surviving predictions. Given a prediction $\hat{b}$ we compute its classification entropy $H(\hat{b}) = -\sum_{c=1}^{C} p_c \cdot \log(p_c)$ and its probability margin score

$$PM(\hat{b}) = (1 - [p_{c_{\max}} - \max_{c \neq c_{\max}} p_c])^2. \qquad (2)$$

Here, $c_{\max}$ denotes the class with the highest probability. We implement dropout layers in order to draw Monte-Carlo (MC) Dropout samples at inference time where activations of the same anchor box $\hat{b}_1, \ldots, \hat{b}_K$ are sampled K times. The final prediction under dropout is the arithmetic mean $\overline{\hat{b}} = \frac{1}{K}\sum_{i=1}^{K} \hat{b}_i$. Moreover, MC mutual information is estimated by

$$MI(\hat{b}) = H(\overline{\hat{b}}) - \overline{H(\hat{b})} \qquad (3)$$

with the second term being the average entropy over MC samples. We also regard the maximum feature standard deviations within $\hat{b}$ by standardizing variances (denoted by $\sigma(\phi) \mapsto \widetilde{\sigma}(\phi)$) over all query predictions to treat localization and classification features on the same footing. The dropout uncertainty is then $D = \max_{\phi \in \hat{b}_{\mathbf{x}}^{(i)}} \widetilde{\sigma}(\phi)$. Note that for all these methods, uncertainty is only considered in the foreground instances. Therefore, either the sum, average, or maximum is taken over predicted instances to obtain a final query score for the image. Summation, for instance, tends to prefer images with a high amount of instances while averaging is strongly biased by the thresholds (e.g., large amounts of false positives could be filtered by a higher threshold).

Additionally, random acquisition serves as a completely uninformed baseline for us. Diversity-based methods make use of latent activation features in neural networks which heavily depend on the OD architecture. Since purely diversity-based methods have been far less prominent in the literature, we focus on the more broadly established uncertainty baselines.

Evaluation. In the literature, methods are frequently evaluated by counting the number of data samples needed to cross some fixed reference performance mark. For OD, performance is usually measured in terms of mAP_{50} (Everingham et al., 2010) for which there is a maximum value $mAP_{50}^{\max}$ known when training on all available data. Some percentage, $0.x \cdot mAP_{50}^{\max}$ needs to be reached with as few data points as possible. Collecting performance over amount of queried data gives rise to curves such as in the top right of Fig. 1, called *AL curves* in the following.

"Amount of training data" usually translates to the number of images which acts as a hyperparameter and is fixed for each method. Considering that each bounding box needs to be labeled and there tends to be high variance in the number of boxes per image in most datasets, it is not clear whether to measure annotated data in terms of images or boxes. Therefore, we stress that the scaling of the t-axis is particularly important in OD. Both views, counting images or boxes, can be argued for. Therefore, we evaluate the performance of each result not only based on images, but also transform the t-axis to the number of annotated boxes. By interpolation between query points and averaging over seeds of the same experiment, we obtain *image- or box-wise error bars* for the performance.

In light of the complexity of the AL problem, we adopt the area under the AL curve (*AUC*). It constitutes a more robust metric compared to horizontal or vertical cross-sections through the learning curves. Figure 2 shows two AL curves on the right and corresponding *AUC* at two distinct points t_1 and t_2. Note that in practice, $mAP_{50}^{\max}$ is not a quantity that is known. Therefore, the AL experiment may be evaluated at any given vertical section of t training data points. Knowing $mAP_{50}^{\max}$ (or the $0.9 \cdot mAP_{50}^{\max}$-mark shown in Fig. 2) *may lead to wrong conclusions* in the presented case which is taken from the scenario in Fig. 5. Ending the experiment at t_1 clearly determines the red curve (which also has a higher *AUC*) as preferable. Ending the experiment at t_2 favors blue by just looking at the current mAP_{50}. However, the *AUC* still favors red, since it takes the complete AL curve into account. This is in line with our qualitative judgement of the curves when regarded up to t_2. We use *AUC* for calculating rank correlations in Section 4.

4 EXPERIMENTS

In this section, we present results of experiments with our sandbox environment as well as established datasets, namely Pascal VOC and BDD100k, in the following abbreviated as VOC and BDD. We do so by presenting AL curves, summarizing benchmark results and discussing our observations for different evaluation metrics. We then show quantitatively that our sandbox results generalize to the same extent to VOC and BDD as results obtained on those datasets generalize between each other. In other words, we demonstrate the *dataset-wise representativity of the results* obtained by our sandbox. Afterwards, this is complemented by a study on the computational speedup achieved.

Table 3: Maximum mAP_{50} values achieved by the models in Table 2 on the respective datasets (standard-size detectors on VOC and BDD; sandbox-size on (E)MNIST-Det). The entire available training data is used.

	YOLOv3	RetinaNet	Faster R-CNN
MNIST-Det	0.962	0.908	0.937
EMNIST-Det	0.959	0.919	0.928
Pascal VOC	0.794	0.748	0.797
BDD100k	0.426	0.464	0.525

Implementation. We implemented our pipeline in the open source MMDetection (Chen et al., 2019) toolbox. In our experiments for VOC, $\mathcal{U}$ initially consists of "2007 train" + "2012 trainval" and we evaluate performance on the "2007 test"-split. When tracking validation performance to assure convergence, we evaluate on "2007 val". Since BDD is a hard detection problem, we filtered frames with "clear" weather condition at "daytime" from the "train" split as initial pool $\mathcal{U}$ yielding 12,454 images. We apply the same filter to the "val" split and divide it in half to get a test dataset (882 images for performance measurement) and a validation dataset (882 images for convergence tracking). For the (E)MNIST-Det datasets we generated 20,000 train images, 500 validation images and 2,000 test images. For reference, we collect in Table 3 the achieved performance of the respective models for each dataset which determines the 90% mark investigated in our experiments.

Benchmark Results. We first investigate differences in AL results w.r.t. the datasets where we fix the detector. This comparison uses the YOLOv3 detector on Pascal VOC, BDD100k and our EMNIST-Det dataset. We investigate the five query methods described in Section 3. We obtain AL curves averaged over four random seeds and evaluated in terms of queried images as well as in terms of queried boxes, respectively. Fig. 5 shows the AL curves with shaded regions indicating point-wise standard deviations obtained by four averaged runs each. The top row shows performance according to queried images while the bottom row shows the same curves but according to queried boxes. We observe that the uncertainty-based query strategies tend to consistently outperform the Random query in image-wise evaluation. However, when regarding the number of queried bounding boxes, the separation vanishes or is far less clear. For EMNIST-Det, the difference between the Random and the uncertainty-based queries decreases substantially, such that only a small difference in box-wise evaluation is visible. For VOC and BDD, the Random baseline falls roughly somewhere in-between the uncertainty baselines in box-wise evaluation. This indicates that greedy acquisition with highest sum of

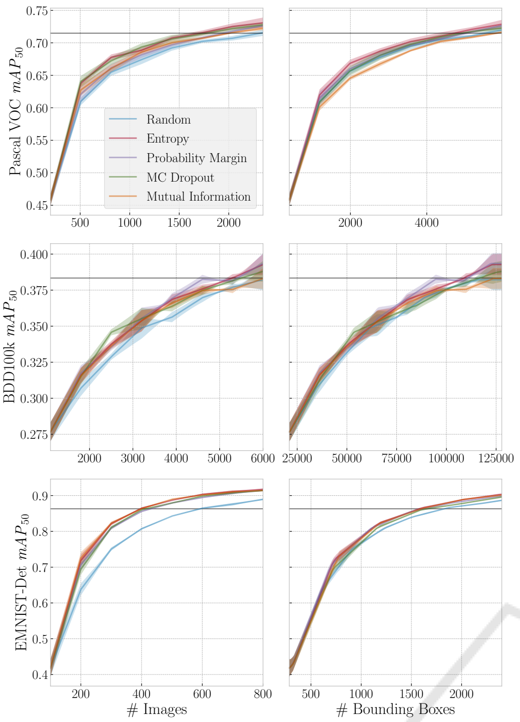

Figure 5: Comparison of YOLOv3 AL curves on three different datasets.

uncertainty tends to prioritize images with a large amount of ground truth boxes. Obtaining a large number of training signals improves detection performance in these cases, while giving rise to a higher annotation cost in the bottom panels. From this observation, *we conclude that comparing AL curves based only on the number images gives an incomplete impression of performance and annotation costs*. Additionally, instance-wise evaluation should be considered. We attribute the smoother curve progression in EMNIST-Det and VOC compared with BDD to the fact that BDD is a far more complicated detection problem with many small objects. However, the AL curve fluctuations on BDD tend to average out in the *AUC* metric. This becomes clear in light of results in the following section, where we study generalization across datasets.

In Table 4 we show additional results. For each detector to reach $0.9 \cdot mAP_{50}^{\max}$, the table shows the number of images required, resp. the number of boxes per method. We see the rankings often favor the Entropy baseline, however, the overall rankings are rather unstable throughout the table. Note in particular, that for (arguably the hardest detection problem) BDD, Random beats the Mutual Information for YOLOv3. The same goes for the experiment using RetinaNet for Pascal VOC. In the analog setting for Faster R-CNN the image-wise margin of the Mutual Information merely becomes slim. This observation also holds for box-wise evaluation and is more pronounced. In six cases, Random beats some informed method. *We conclude that in order to assess the viability of a method, AL curves should be viewed from both angles: performance over number of images and over number of boxes queried.*

Generalization of Sandbox Results. Instead of evaluating the pure performance at each AL step we have proposed computing the corresponding *AUC* as a more robust metric of AL performance. With respect to the final method ranking at $mAP_{50}^{\max}$, we compute Spearman rank correlations with the mAP_{50} metric at each point t. We compare these with the analogous correlations with the respective *AUC* at each point. Fig. 6 shows intensity diagrams representing the rank correlations both, in terms of image-wise and box-wise evaluation. The t-axes are normalized to the maximum number of images, resp. bounding boxes queried, color indicates the Spearman correlation of the rankings. In Fig. 6 both, mAP_{50} and *AUC* show overall high correlation with the method ranking, especially towards the end of the curves. We see that the correlations for *AUC* fluctuates far less. Moreover, the average correlation across entire AL curves tends to be larger for *AUC* than mAP_{50}. Note that the final ranking of either method does not need to be perfectly correlated with the $mAP_{50}^{\max}$-ranking for two reasons. Firstly, the latter does not take into consideration early performance gains and secondly, the $mAP_{50}^{\max}$-ranking is a horizontal section through the curves while mAP_{50} and *AUC* are vertical sections. We *conclude that AUC tends to be highly correlated with the $mAP_{50}^{\max}$-ranking and is more stable w.r.t. t than mAP_{50}.*

Next, we study comparability of AL experiments between the sandbox setting and full-complexity problems (VOC and BDD). To this end, we consider the cross-dataset correlations of the *AUC* score when fixing the detection architecture. Fig. 7 shows correlation matrices for image- and instance-wise evaluation on the left for the YOLOv3 detector. VOC-BDD correlations tend to be similar to EMNIST-Det-VOC and EMNIST-Det-BDD correlations in image-wise evaluation. However, when correcting for variance in instance-count per image in box-wise evaluation on the right, we find correlations are generally high. In particular, results for BDD and VOC are roughly equally correlated with results on any other dataset. We conclude that *comparing methods in the simplified setting yields a similar amount of information about relative performances of AL as the full-complexity setting*.

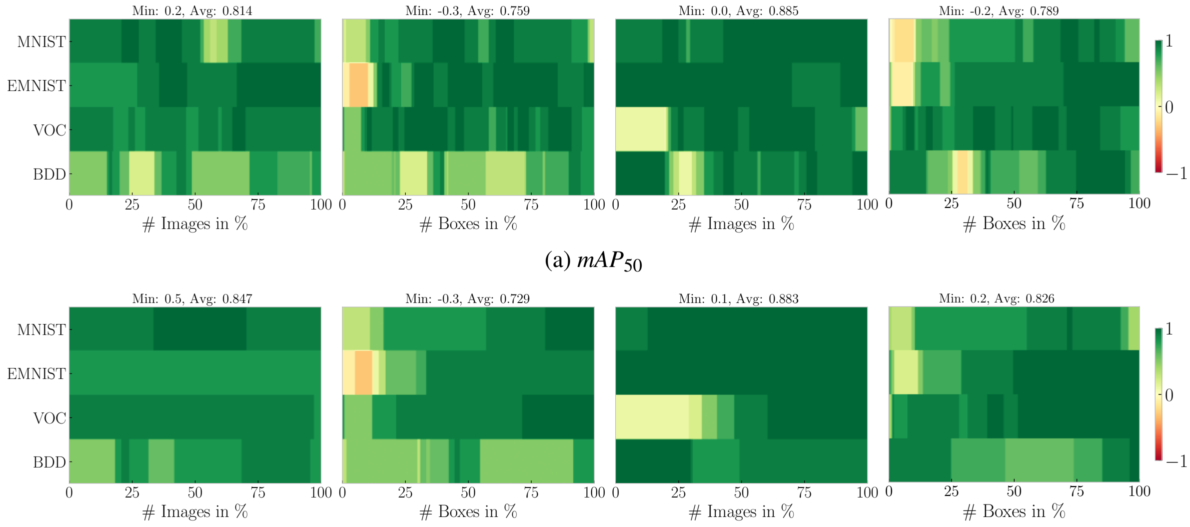

(a) mAP_{50}

(b) *AUC*

Figure 6: Intensity diagrams of rank correlations between the mAP_{50}, resp. cumulative *AUC* and the final rankings obtained at the $0.9 \cdot mAP_{50}^{\max}$-mark. Left: YOLOv3; Right: Faster R-CNN.

Table 4: Amount of queried images and bounding boxes necessary to cross the 90% performance mark during AL. Lower values are better. Bold numbers indicate the lowest amount of data per experiment and underlined numbers are the second lowest.

		# queried images				# queried bounding boxes			
		MNIST-Det	EMNIST-Det	Pascal VOC	BDD100k	MNIST-Det	EMNIST-Det	Pascal VOC	BDD100k
YOLOv3	Random	327.9	595.6	2236.8	5871.2	1079.1	1825.3	5344.2	116362.1
	Entropy	**245.5**	**398.8**	1732.8	5389.3	**1004.9**	**1583.0**	**4695.4**	110694.9
	Prob. Margin	256.2	429.0	1858.5	**4895.2**	1013.7	1617.1	4787.6	**100376.3**
	MC Dropout	256.3	416.2	**1679.4**	5200.5	1115.3	1671.6	4875.1	110427.6
	Mutual Inf.	249.8	399.5	1884.2	5912.9	1061.9	1602.7	5527.0	125050.1
Faster R-CNN	Random	450.0	843.4	1293.7	6434.3	2140.0	2891.7	3125.2	129219.0
	Entropy	**384.5**	**561.6**	**1030.6**	5916.7	**1608.4**	**2156.4**	**2707.0**	123008.6
	Prob. Margin	408.7	626.2	1036.5	**5761.6**	1622.9	2285.1	2711.6	**117889.3**
	MC Dropout	390.5	647.4	1127.5	6296.4	1818.1	2773.8	3624.7	130533.8
	Mutual Inf.	395.3	572.6	1080.2	6385.7	1695.6	2235.3	3026.5	132855.7
RetinaNet	Random	390.3	950.4	2555.4	3616.2	1283.8	2957.7	6220.0	69842.0
	Entropy (sum)	**288.6**	**687.7**	**1961.2**	**2866.5**	1292.0	2708.6	**5421.6**	64939.7
	Prob. Margin (sum)	310.8	733.9	2087.3	2901.5	1277.5	2721.5	5445.6	64794.9
	MC Dropout (sum)	293.3	749.6	2745.3	3027.7	1317.4	2926.4	7047.9	62395.5
	Mutual Inf. (sum)	289.6	719.0	2881.9	3124.9	**1248.0**	**2677.4**	7389.0	**61712.9**

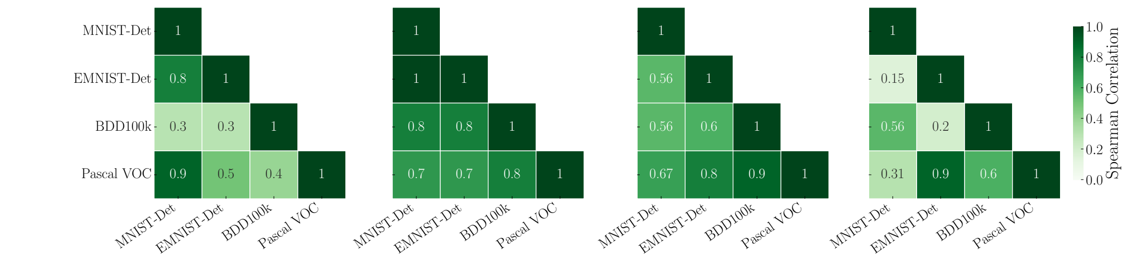

(a) YOLOv3

(b) Faster R-CNN

Figure 7: Ranking correlations between *AUC* values for YOLOv3 and Faster R-CNN. Left: Image-wise; Right: Instance-wise evaluation.

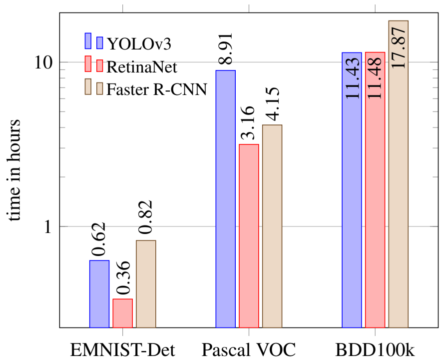

Figure 8: Utilized time for one AL step (training to convergence + query evaluation) for investigated settings in hours.

Compute Time. AL for advanced image perception tasks tends to be highly time intensive, compute-heavy and energy consuming. This is due to the fact that at each AL step the model should be guaranteed to fit to convergence and there are multiple steps of several random seeds to be executed. Fig. 8 on the right shows the time per AL step used in our setting when run on a Nvidia Tesla V100-SXM2-16GB GPU with a batch size of four. The time-axis is scaled logarithmically, so the experiments on EMNIST-Det are always faster by at least half an order of magnitude. Training of YOLOv3 on VOC does not start from COCO-pretrained weights (like YOLOv3+BDD) since the two datasets VOC and COCO are highly similar. In this case, we opt for an ImageNet (Russakovsky et al., 2015)-pretrained backbone like for the other detectors. Overall, we save time up to a factor of around 14 for VOC and around 32 for the BDD dataset. *Translated to AL investigations, this means that the effects of new query strategies can be evaluated within half a day* on a single Nvidia Tesla V100-SXM2-16GB.

5 CONCLUSION

In this work, we investigated the possibility of simplifying the active learning setting in object detection to accelerate development and evaluation. We found that for a given detector, active learning results, in particular on instance level, generalize well between different datasets, including (E)MNIST-Det. Particularly, we find a representative degree of result comparability between our sandbox datasets and full-complexity active learning. In our evaluation, we included a more direct measurement of annotation effort in counting the number of boxes in addition to queried images. Meanwhile, we can save more than an order of magnitude in total compute time by the down-scaling of the detector and reducing the dataset complexity. Our environment allows for consistent benchmarking of active learning methods in a unified framework, thereby improving transparency. We hope that the present sandbox environment, findings and configurations along with the implementation will lead to further and accelerated progress in the field of active learning for object detection.

ACKNOWLEDGMENTS

The research leading to these results is funded by the German Federal Ministry for Economic Affairs and Climate Action" within the projects "KI-Absicherung - Safe AI for Automated Driving", grant no. 19A19005R and "KI Delta Learning - Scalable AI for Automated Driving", grant no. 19A19013Q as well as by the German Federal Ministry for Education and Research within the project "UnrEAL" grant no. 01IS22069. We thank the consortia for the successful cooperation. We gratefully acknowledge financial support by the state Ministry of Economy, Innovation and Energy of Northrhine Westphalia (MWIDE) and the European Fund for Regional Development via the FIS.NRW project BIT-KI, grant no. EFRE-0400216. The authors gratefully acknowledge the Gauss Centre for Supercomputing e.V. for funding this project by providing computing time through the John von Neumann Institute for Computing on the GCS Supercomputer JUWELS at Jülich Supercomputing Centre.

EUROPEAN UNION
Investing in our Future
European Regional
Development Fund

REFERENCES

Bouguelia, M.-R., Belaïd, Y., and Belaïd, A. (2015). Identifying and mitigating labelling errors in active learning. In *International Conference on Pattern Recognition Applications and Methods*, pages 35–51. Springer.

Bouguelia, M.-R., Nowaczyk, S., Santosh, K., and Verikas, A. (2018). Agreeing to disagree: Active learning with noisy labels without crowdsourcing. *International Journal of Machine Learning and Cybernetics*, 9(8):1307–1319.

Brust, C.-A., Käding, C., and Denzler, J. (2018). Active learning for deep object detection. *arXiv preprint arXiv:1809.09875*.

Budd, S., Robinson, E. C., and Kainz, B. (2021). A survey on active learning and human-in-the-loop deep learning for medical image analysis. *Medical Image Analysis*, 71:102062.

Chen, K., Wang, J., Pang, J., Cao, Y., Xiong, Y., Li, X., Sun, S., Feng, W., Liu, Z., Xu, J., Zhang, Z., Cheng, D., Zhu, C., Cheng, T., Zhao, Q., Li, B., Lu, X., Zhu, R., Wu, Y., Dai, J., Wang, J., Shi, J., Ouyang, W., Loy, C. C., and Lin, D. (2019). MMDetection: Open mmlab detection toolbox and benchmark. *arXiv preprint arXiv:1906.07155*.

Choi, J., Elezi, I., Lee, H.-J., Farabet, C., and Alvarez, J. M. (2021). Active learning for deep object detection via probabilistic modeling. In *Proceedings of the IEEE/CVF International Conference on Computer Vision*, pages 10264–10273.

Cohen, G., Afshar, S., Tapson, J., and Van Schaik, A. (2017). Emnist: Extending mnist to handwritten letters. In *2017 international joint conference on neural networks (IJCNN)*, pages 2921–2926. IEEE.

Desai, S. V., Lagandula, A. C., Guo, W., Ninomiya, S., and Balasubramanian, V. N. (2019). An adaptive supervision framework for active learning in object detection. In Sidorov, K. and Hicks, Y., editors, *Proceedings of the British Machine Vision Conference (BMVC)*, pages 177.1–177.13. BMVA Press.

Elezi, I., Yu, Z., Anandkumar, A., Leal-Taixé, L., and Alvarez, J. M. (2022). Not all labels are equal: Rationalizing the labeling costs for training object detection. In *Proceedings of the IEEE/CVF Conference on Computer Vision and Pattern Recognition (CVPR)*, pages 14492–14501.

Everingham, M., Van Gool, L., Williams, C. K. I., Winn, J., and Zisserman, A. (2010). The pascal visual object classes (voc) challenge. *International Journal of Computer Vision*, 88(2):303–338.

Gal, Y. and Ghahramani, Z. (2016). Dropout as a bayesian approximation: Representing model uncertainty in deep learning. In *international conference on machine learning*, pages 1050–1059. PMLR.

Gal, Y., Islam, R., and Ghahramani, Z. (2017). Deep bayesian active learning with image data. In *International Conference on Machine Learning*, pages 1183–1192. PMLR.

Haussmann, E., Fenzi, M., Chitta, K., Ivanecky, J., Xu, H., Roy, D., Mittel, A., Koumchatzky, N., Farabet, C., and Alvarez, J. M. (2020). Scalable active learning for object detection. In *2020 IEEE intelligent vehicles symposium (iv)*, pages 1430–1435. IEEE.

LeCun, Y., Bottou, L., Bengio, Y., and Haffner, P. (1998). Gradient-based learning applied to document recognition. *Proceedings of the IEEE*, 86(11):2278–2324.

Li, M. and Sethi, I. K. (2006). Confidence-based active learning. *IEEE transactions on pattern analysis and machine intelligence*, 28(8):1251–1261.

Lin, T.-Y., Goyal, P., Girshick, R., He, K., and Dollár, P. (2017). Focal loss for dense object detection. In *Proceedings of the IEEE international conference on computer vision*, pages 2980–2988.

Lin, T.-Y., Maire, M., Belongie, S., Hays, J., Perona, P., Ramanan, D., Dollár, P., and Zitnick, C. L. (2014). Microsoft coco: Common objects in context. In *European conference on computer vision*, pages 740–755. Springer.

Netzer, Y., Wang, T., Coates, A., Bissacco, A., Wu, B., and Ng, A. Y. (2011). Reading digits in natural images with unsupervised feature learning.

Papadopoulos, D. P., Uijlings, J. R., Keller, F., and Ferrari, V. (2017). Training object class detectors with click supervision. In *Proceedings of the IEEE Conference on Computer Vision and Pattern Recognition*, pages 6374–6383.

Redmon, J. and Farhadi, A. (2018). Yolov3: An incremental improvement. *arXiv preprint arXiv:1804.02767*.

Ren, S., He, K., Girshick, R., and Sun, J. (2015). Faster r-cnn: Towards real-time object detection with region proposal networks. *Advances in neural information processing systems*, 28.

Roy, S., Unmesh, A., and Namboodiri, V. P. (2018). Deep active learning for object detection. In *BMVC*, page 91.

Russakovsky, O., Deng, J., Su, H., Krause, J., Satheesh, S., Ma, S., Huang, Z., Karpathy, A., Khosla, A., Bernstein, M., Berg, A. C., and Fei-Fei, L. (2015). ImageNet Large Scale Visual Recognition Challenge. *International Journal of Computer Vision (IJCV)*, 115(3):211–252.

Schmidt, S., Rao, Q., Tatsch, J., and Knoll, A. (2020). Advanced active learning strategies for object detection. In *2020 IEEE Intelligent Vehicles Symposium (IV)*, pages 871–876. IEEE.

Settles, B. (2009). Active learning literature survey. Computer Sciences Technical Report 1648, University of Wisconsin–Madison.

Subramanian, A. and Subramanian, A. (2018). One-click annotation with guided hierarchical object detection. *arXiv preprint arXiv:1810.00609*.

Tsvigun, A., Shelmanov, A., Kuzmin, G., Sanochkin, L., Larionov, D., Gusev, G., Avetisian, M., and Zhukov, L. (2022). Towards computationally feasible deep active learning. In Carpuat, M., de Marneffe, M.-C., and Meza Ruiz, I. V., editors, *Findings of the Association for Computational Linguistics: NAACL 2022*, pages 1198–1218, Seattle, United States. Association for Computational Linguistics.

Yoo, D. and Kweon, I. S. (2019). Learning loss for active learning. In *Proceedings of the IEEE/CVF conference on computer vision and pattern recognition*, pages 93–102.

Younesian, T., Epema, D., and Chen, L. Y. (2020). Active learning for noisy data streams using weak and strong labelers. *arXiv preprint arXiv:2010.14149*.

Younesian, T., Zhao, Z., Ghiassi, A., Birke, R., and Chen, L. Y. (2021). Qactor: Active learning on noisy labels. In *Asian Conference on Machine Learning*, pages 548–563. PMLR.

Yu, F., Chen, H., Wang, X., Xian, W., Chen, Y., Liu, F., Madhavan, V., and Darrell, T. (2020). Bdd100k: A diverse driving dataset for heterogeneous multitask learning. In *Proceedings of the IEEE/CVF conference on computer vision and pattern recognition*, pages 2636–2645.

Yuan, T., Wan, F., Fu, M., Liu, J., Xu, S., Ji, X., and Ye, Q. (2021). Multiple instance active learning for object detection. In *Proceedings of the IEEE/CVF Conference on Computer Vision and Pattern Recognition*, pages 5330–5339.

Zhan, X., Wang, Q., Huang, K.-h., Xiong, H., Dou, D., and Chan, A. B. (2022). A comparative survey of deep active learning. *arXiv preprint arXiv:2203.13450*.